Optical Fibre Sensors for Earth Sciences: from Basic Concepts to Optimising Glass Composition for High Temperature Applications

G. Brambilla, H.H. Kee, V. Pruneri*, and T.P. Newson

Optoelectronics Research Centre, University of Southampton, Southampton, SO17 1BJ, UK

Tel: ++44-(0)23-8059-3954, Fax: ++44-(0)23-8059-3149, GB2@ORC.SOTON.AC.UK

**Now with O.T.I.-Corning, viale Sarca 222, Milano, Italy*

Abstract:

This paper reviews the technical evolution of optical fibre sensors relevant to earth sciences with particular reference to high temperature measurements. Optimisation of fibre composition and system design to fully realise the potential of these sensors has led to the substantial advances in both distributed and point sensor systems. Applications of these sensors in the field of earth sciences are discussed to provide a deeper understanding of the potential for monitoring geodynamical and chemical processes in areas of high seismic and volcanic risk.

1. Introduction

In the last two decades, optical fibre sensors have attracted much attention because of their many potential applications. The state of the art allows the measurement of a large number of physical quantities, including temperature, pressure, chemical quantities, flow, liquid level, position, displacement, electric and magnetic fields, vibration, rotation and pH. Moreover, optical fibre sensors can be integrated with optical fibre communication systems to provide remote sensing capabilities. In fact optical fibres have an extremely low propagation loss (~0.2dB/Km at 1.5 μm) and the signal can propagate tens or even hundreds of Km into the fibre before excessive degradation occurs. Earth science can benefit from the most recent developments in the optical fibre sensors field to measure physical quantities in remote places which would otherwise remain inaccessible, for example cracks in the rock, in adverse environments saturated with dangerous chemical compounds or simply in geological sites far from the observation laboratory such as volcanoes or deep oceans. Fibre optics can also be used as a light carrier for a

remote or microscopic light source or camera. The Optoelectronics Research Centre at Southampton University has a particular interest in the state of the art fibre Bragg gratings providing high temperature capabilities and also Brillouin scattering for distributed strain and temperature sensing.

2. Fibre sensors

As previously observed, there is a myriad of optical fibre sensors. They can be grouped in three categories according to the means of sensing, the extent of sensing and the role of optical fibres. As far as the means of sensing is concerned, sensors are grouped as intensity sensors or interferometric sensors according to whether they are based on intensity or phase changes. Intensity sensors include devices based on scattering (Rayleigh, Brillouin or Raman), attenuation (losses added by fibre bending or induced absorption), and change in mode propagation inside the fibre. Interferometric sensors are based on monitoring phase induced changes arising from changes in optical path length which may arise from various physical phenomena. The classification based on extent of sensing groups devices as distributed or "point" sensors. While distributed sensors detect changes of physical quantities continuously along the fibre length, in point sensors the device is sensitive over a limited distance. Finally, sensors are classified as intrinsic or extrinsic sensors depending on whether the device is the fibre itself or the fibre merely serves to transport the signal. Examples of intrinsic sensors are devices based on bending losses to measure pressure or on attenuation in modified cladding to detect chemicals. Absorption cells to measure chemicals through spectroscopic analysis are examples of extrinsic sensors. In the following sections we describe a few examples of intensity distributed or point sensors that can be used to detect chemicals, temperature, pressure, strain, displacement and position.

3. Distributed sensors

Distributed fibre sensing has been extensively researched, and systems operating in the 1.5 μm wavelength region are particularly beneficial for long range measurements due to the low intrinsic signal attenuation of the optical fibre in this wavelength region. Additionally, silica fibres unrivalled capability to provide measurement of the property of interest as a continuous function of linear position along the sensing fibre has increased its importance in the arena of optical fibre sensors. Distributed sensors were initially demonstrated for use in fault location and loss distribution measurements [1], and subsequently for other measurands such as temperature, strain or even chemical sensing [2]. In the field of volcanic/seismic measurements, distributed sensors will prove to be beneficial for fibre, temperature and strain measurements encompassing a vast geographical domain.

Several different schemes have been demonstrated for realising distributed sensors, those using Rayleigh, Raman or Brillouin scattering mechanisms that will be discussed in the next section. Distributed sensors may also be classified as single-ended sensors utilising spontaneous scattering, or sensors requiring access to both ends of the sensing fibre utilising the stimulated scattering mechanism. Although there is more detected signal available using the stimulated scattering scheme, this technique is generally unsuitable for many applications, where only a single end of the sensing fibre is accessible.

One popular method for single-ended distributed sensing measurements is using the optical time domain reflectometry (OTDR) technique that was first demonstrated in 1976 by Barnowski and Jensen [3]. Using the powerful OTDR principle, a pulse of light is transmitted down the fibre and the light which is backscattered within the numerical aperture of the fibre is measured. The time between sending the pulse of light and detecting the backscattered signal provides a measure of the distance along the fibre whilst the intensity of the backscattered light provides the information of the measurand.

3.1 Scattering mechanims

The different scattering mechanisms in optical fibres and their dependencies on various measurands can be classified into that of Rayleigh, Raman and Brillouin scattering. Rayleigh scattering results from random inhomogeneities of the density and compositional variations that are frozen into optical fibres during the manufacturing process. These variations cause refractive index fluctuations, resulting in a fraction of the scattered light lying within the numerical aperture of the fibre being guided in the opposite direction to that of the incident light. It is an elastic scattering mechanism because there is no difference in the frequency between that of the incident light and the backscattered light. Rayleigh scattering is an intrinsic loss mechanism, and in the low-loss wavelength region of an optical fibre, Rayleigh scattering forms the dominant loss of light passing through the fibre. In an OTDR sensor, the backscattered light decays exponentially with distance/time as the pulse travels down the sensing fibre due to Rayleigh scattering. This backscattered power detected back at the input of the fibre as a function of time t is given by the relation [4]:

$$P_R = \frac{1}{2} P_{in} W_o \gamma_R \upsilon_g S\left(\exp^{-\upsilon_g \gamma_R t}\right) \qquad (1)$$

where P_{in} is the input optical power, W_o is the input pulse width, υ_g is the group velocity of the pulse in the fibre, γ_R is the Rayleigh scattering coefficient and S is the capture fraction of the backscattered signal within the numerical aperture.

OTDR systems based on Rayleigh scattering have been successfully exploited commercially as a fibre diagnostic tool for the detection of fibre attenuation and damage. However, with conventional silica fibres as the sensing element, these systems are unable to perform measurements related to measurands such as strain and temperature.

Raman scattering is an inelastic scattering mechanism that occurs during the excitation of vibrational modes in the optical fibre. The peak of Raman gain in fused silica occurs at 440 cm^{-1} (approximately 13 THz for the pump wavelength of 1.5 μm) away from the wavelength of the incident light [5]. In silica glass, Raman scattering occurs over a wide range of frequencies. This is due to the fact that the molecules in a glass lattice are non-crystalline or amorphous in nature, leading to different vibrational energies for different groups of molecules within the glass structure. The probability of the anti-Stokes Raman scattering is smaller than the Stokes scattering because the scattering occurs from molecules in an excited state, which will have a lower population. This results in a smaller backscattered power than the corresponding Stokes Raman scattering.

The approach based on Raman scattering has been successfully exploited commercially for performing distributed temperature measurements, due to the ease of using conventional silica-based optical fibres as the sensing element and availability of high performance wavelength selective filters. However, there has been intensive research recently into distributed sensors using Brillouin scattering, as this technique may be applied to perform simultaneous strain and temperature measurements. This is possible since both the Brillouin frequency shift and intensity are dependent on strain and temperature and overcomes the previous major obstacle of fibre sensors which was the crosstalk resulting from multiple physical phenomena such as strain and temperature. By measuring both the Brillouin intensity and frequency shift along the sensing fibre, the information relating to temperature and/or strain may be unambiguously resolved.

Spontaneous Brillouin scattering occurs when a small fraction of incident light is inelastically scattered by thermally excited acoustic waves (acoustic phonons) in the optical fibre. A periodic modulation of the dielectric constant and hence the refractive index of the medium is generated due to density variations produced by the acoustic wave. The

scattered light then experiences a Doppler shift in frequency and has maximum scattering in the backwards direction, whereby this frequency is expressed as:

$$\nu_B = \frac{2n\nu_a}{\lambda_p} \tag{2}$$

where n is the refractive index, ν_a is the acoustic velocity, and λ_p is the pump wavelength. The Brillouin frequency shift is approximately three orders of magnitude smaller than that for Raman scattering, due to the much smaller acoustic phonon frequencies involved in the process of Brillouin scattering (~11 GHz for a pump wavelength at 1.5 μm). This results in the need for a narrowband and efficient filter to sufficiently separate the Brillouin from the Rayleigh signal.

The variation in Brillouin frequency shift $\Delta\upsilon_B$ and intensity ΔP_B due to strain $\Delta\varepsilon$ and temperature ΔT may be related by the matrix equation:

$$\begin{bmatrix} \Delta\upsilon_B \\ \Delta P_B \end{bmatrix} = \begin{bmatrix} C_{\upsilon_B\varepsilon} & C_{\upsilon_B T} \\ C_{P_B\varepsilon} & C_{P_B T} \end{bmatrix} \begin{bmatrix} \Delta\varepsilon \\ \Delta T \end{bmatrix} \tag{3}$$

where $C_{P_B\varepsilon}$ and $C_{P_B T}$ are the intensity coefficients for strain and temperature, and $C_{\upsilon_B\varepsilon}$ and $C_{\upsilon_B T}$ are the frequency coefficients for strain and temperature respectively. By taking the inverse matrix, the independent parameters of strain and temperature can be resolved provided that the determinant of the inverse matrix has a non-zero value:

$$\begin{bmatrix} \Delta\varepsilon \\ \Delta T \end{bmatrix} = \frac{1}{\left| C_{\upsilon_B\varepsilon} C_{P_B T} - C_{P_B\varepsilon} C_{\upsilon_B T} \right|} \begin{bmatrix} C_{P_B T} & -C_{\upsilon_B T} \\ -C_{P_B\varepsilon} & C_{\upsilon_B\varepsilon} \end{bmatrix} \begin{bmatrix} \Delta\upsilon_B \\ \Delta P_B \end{bmatrix} \tag{4}$$

The next section provides experimental evidence of simultaneous distributed strain and temperature measurements based on spontaneous Brillouin scattering and demonstrating the use of in-fibre optical Mach-Zehnder interferometers as an optical filter and for the Brillouin frequency shift discrimination.

3.2 Simultaneous Strain and Temperature Measurement

The experimental configuration of the sensing system comprises five main components, the amplified narrow linewidth laser source illustrated in figure 1(a), the sensing fibre, the Mach-Zehnder interferometers, a broadband Q-switched laser source used to obtain the Rayleigh signal and the detection and averaging systems shown in figure 1(b). To generate the required high peak power, a narrow linewidth source, continuous wave (CW) semiconductor distributed feedback (DFB) laser with an output power of 2.5 mW, was used. This was externally modulated by a

$LiNbO_3$ electro-optic modulator (EOM) and amplified using an Erbium-doped fibre amplifier (EDFA1) with 26 dB gain, and the residual amplified spontaneous emission (ASE) noise was filtered by a in-fibre Bragg grating (Reflectivity = 99.4 %, $\Delta\lambda$ = 0.08nm, λ = 1533.4 nm). The reflected signal was then amplified using another EDFA (EDFA2) to overcome the loss of the acousto-optic modulator (AOM) which served to gate the pulse and filter the ASE generated by the second EDFA. The resultant signal pulse had a peak power of 1.6 W, pulse width of 30ns and spectral linewidth of <100 MHz. The AOM is synchronised with the EOM and pulses are generated at a repetition rate of 6600 Hz. The signal was passed through a 95/5 fibre coupler (FC1), 5 % of the signal was used to control the optical filters and the remaining signal power was then launched into the sensing fibre via another circulator (C2) as shown in figure 1(b).

The sensing fibre consisted of 15 km of conventional telecommunications grade single- mode silica fibre. The first length of sensing fibre was a 9 km drum (D1), followed a section of 0.46 km drum D2. Fibre drum D2 was placed in an oven and subjected to a temperature of 53 °C, an increase in temperature of 30°C from the temperature from other drums of fibre at room temperature (23 °C). Drums D4 and D5 consisted of a continuous length of fibre. Between D4 and D5 there was a 120 m section of fibre which was loosely reeled on to 11 pairs of pulleys. Weights were then added on one of the ends of the 120 m length of fibre to provide a strain. The change in length of the fibre was measured and to determine the average strain over the 120 m, the backscattered signal was collected through the circulator (C2) and filtered through the two cascaded Mach-Zehnder interferometers.

The first in-fibre Mach-Zehnder (MZ1) was used in a double-pass configuration with a path imbalance of 9.2 mm (FSR = 22 GHz) introduced between the two arms of the interferometer. This provided maximum rejection of the Rayleigh signal from the Brillouin to minimise the effect of coherent Rayleigh noise (CRN) [6] which has a detrimental effect on the strain and temperature resolution. The output of this first Mach-Zehnder was then fed through to the second Mach-Zehnder (MZ2) which was in a single-pass configuration and with a path imbalance of 28.6 mm (FSR = 7 GHz). The second Mach-Zehnder was used to convert the Brillouin frequency shift to an intensity change. As the Brillouin intensity may be measured independently of frequency through tuning the second Mach-Zehnder and obtaining two separate output signals [7], the Brillouin frequency shift can also be calculated.

The backscattered traces were obtained from the output of the single pass Mach-Zehnder using a InGaAs photo-detector and a preamplifier which has a sensitivity of 10 mV/nA and an electrical bandwidth of 3 MHz. The

backscattered traces were averaged 65536 times with an averaging time of 15 minutes. The attenuation and splice/bend losses are compensated for by dividing the Brillouin signals by the Rayleigh signal, and this is known as the Landau-Placzek ratio. Known constants relating the Brillouin frequency shift and intensity to strain and temperature were used in conjunction with the sets of data obtained to solve two simultaneous equations to produce strain and temperature profiles [8], as shown in figure 2(a) and figure 2(b). The temperature resolution and strain resolutions were estimated from the r.m.s noise of the signals to be 4 °C and 290 με with a spatial resolution of 10 m. The slope on the strained region is due to friction on the pulleys.

3.3 Recent progress in distributed sensing using Brillouin scattering

With the success of the initial demonstration of simultaneous strain and temperature sensing, the spontaneous Brillouin-based system has recently been refined to using the technique of microwave heterodyne detection. This method employs a narrow linewidth optical local oscillator signal that mixes with the Brillouin backscattered signal and allows excellent electrical filtering of the Brillouin component from the Rayleigh signal rather than the Mach-Zehnder optical filters, as well as achieving a greater dynamic range. Distributed temperature measurements over a 57 km length of sensing fibre (comprising five separate lengths of 17.5 km, 17.5 km, 17.5 km, 0.5 km and 4 km, with the drum of 500 m being placed in an oven) was obtained, the longest sensing length yet presented using single-ended detection of spontaneous Brillouin backscatter [9]. The Brillouin frequency shift with its linear dependence on temperature variation is shown in figure 3.

At the other extreme of very short spatial resolution measurements, there is a need for fine monitoring for some applications. Several methods for temperature sensing using Raman scattering have been proposed in the past, which achieved metre-order spatial resolution. In the case of Brillouin scattering, a novel method using direct-frequency-modulation of a tuneable laser diode and electro-optic modulator (EOM) demonstrated a spatial resolution of 45 cms for a 7.8-metre sensing range [10]. Using single-ended spontaneous Brillouin OTDR, distributed temperature measurements down to an accuracy of 35 cm spatial resolution has been demonstrated utilising conventional single-mode silica fibres for a range of 1 km [11].

3.4 Remote sensing

A significant feature of distributed fibre sensors is the capability to perform remote sensing which is advantageous for geodynamical monitoring of areas with high volcanic risk. In such a situation, a portion of the conventional telecommunications single-mode optical fibre may function as the passive medium to form a link between the

source/detection system and volcanic vicinity, and the remaining length as the sensing element itself. One possible method to increase the dynamic range of such OTDR systems is through optical amplification, either within the sensing fibre by amplifying the signal pulse [12], or through amplification of the backscattered signal [9]. Distributed fibre sensors have also successfully exploited the commercial interest of borehole monitoring for oil and gas reservoirs, for the last decade, using Raman backscatter which is temperature-sensitive [13]. The technological advances and functionality of such systems may similarly be useful for borehole temperature monitoring within areas with potential volcanic activities for a greater understanding the earth's interior processes.

4. Point sensors

Point sensors are devices that modify the fibre transmission properties within a limited spatial region. This can be achieved with an external device applied to the fibre or it can be internal to the fibre itself. The former group incorporates devices such as moving diaphragms or silicon membrane for pressure sensing, fluorescent phosphors for temperature sensing, spectroscopic cells for chemical sensing, piezoelectric or "piezomagnetic" materials for electrical and magnetic sensing. Examples of intrinsic devices are clamps that induce microbending in the fibre, evanescent wave sensors (EWS) and fibre Bragg gratings (FBG). EWS are devices that use perturbations of the evanescent wave in the propagation mode as a means of sensing. FBGs are periodical modifications in the core refractive index that act as selective reflectors. The wavelength of the maximum reflection (called Bragg wavelength λ_B) shifts when the fibre dilates or shrinks and is used to sense the physical effects that induce such modifications. Devices produced using FBG have high mechanical and chemical reliability and can be use in the most adverse environments. Another major advantage is that FBG can be arranged in arrays and multiplexed, thus allowing the simultaneous measurement of several different physical parameters in different parts of the same fibre.

4.1 Extrinsic sensing

- Pressure and position

One group of extrinsic devices is based on backreflection from a movable diaphragm which may be sensitive to either pressure or acceleration [14,15]. If a silicon membrane is anodically bonded to the end of the fibre as a reflecting surface [16], device dimensions are considerably reduced. Silicon membrane devices can measure pressure differences as little as few percents and can be monitored using at least two wavelengths to avoid competing effects like temperature. When a conical tip is used as an end-face mirror [17], light is totally reflected if the fibre is surrounded by air and it is only partially reflected from the fibre if the fibre is inserted in a liquid with a higher

refractive index. If the liquid refractive index matches the fibre refractive index, none of the injected light is reflected. These devices are used to measure displacements of liquid surfaces and they are thus referred to as liquid level sensors. Permanently installed sensors located deep sub surface can be used to constantly monitor the level of natural underground reservoirs.

- Temperature

There are many techniques used for thermometry: fluorescence emission, Fabry-Perot interferometers and remote pyrometers. The first method is based on the measurement of the fluorescent emission decay of rare earth doped or transition metal doped phosphors. Cr:YAG [18] and Yttrium oxides and Yttrium orthovanadate activated with Eu [19] allow measurements in the range 25-500 and 500-1000 ^{o}C, respectively. These devices need an exciting source at a selected wavelength and a detector with monochromator to select the fluorescence of the activated transition. Fabry-Perot interferometers measure the change of optical path in materials (like ZnSe or calcite) whose expansion coefficient and refractive index are known as a function of the temperature. As previously explained in the case of silicon membrane, many wavelengths can be used to compensate for pressure changes or other effects. The third technique considered, remote pyrometry, is based on the detection of blackbody radiation from small samples of sapphire placed in contact with the body to analyse. This technique might be extremely useful for high temperature applications like in volcanic areas.

- Chemicals

Spectroscopic analysis of gases can be performed by positioning a mirror with focusing optics at the end of the fibre and analysing the absorption spectrum. A cell 8 cm long allows the measurement of methane concentration via its absorption at 1.66 μm (first overtone of the fundamental in the infrared) [20]. With a multi-wavelength source it is also possible to detect particulates and their concentration [21]. An opto-supplying technique can be used to move the working wavelength to the near infrared, where the silicate fibre absorption is lower. For example a CO_2 spectroscopic sensor changes the working wavelength from 4.3 μm (where the fundamental vibrational mode is) to 860 nm [22]. Specific chemical sensors can be produced using chemical sensitive materials. For example Au on Co_3O_4 is a catalyst used for CO detection [23]. A fluorescent sodium ion carrier can be used as Na sensors in the concentration range from $2*10^{-5}$ to 10^{-1} mol/l [24]. Hydroxypyrene trisulfonate and a suspension of metal-organic compounds are used as fluorescent elements for CO_2 and oxygen detection [25]. These fluorescent compounds are

excited by visible light and can be used together in the same fibre. The chemical to detect can also be a fluorescence quencher, like sulphur dioxide for benzo(b)fluoranthene. [26]. These sensors can be arrayed to detect simultaneously many chemical species. The use of new generations of infrared transparent fibre materials such as chalcogenides and halides extends the optical window utilisable for chemical sensing systems considerably in the middle infrared region, where most of the vibrational and rotational transitions occur [27]. Finally field measurements have been done using a spectrometer equipped with two distributed feedback semiconductor lasers resonant with CO_2 and H_2O [28]. Coupling with optical fibres allows the remote operation of the device for continuous monitoring and surveillance of volcanic areas.

Vibration

One of the common techniques for vibration sensing is based on intrinsic sensing. The basic configuration consists of a coil of fibre wrapped on a compliant cylinder that held a seismic mass in place [29]. The two coils represent the two arms of a Michelson interferometer. When the accelerometer is subject to vibrations, one cylinder is compressed and the other is stretched. The fibre is consequently stretched and this can be detected as an optical phase shift. Hydrophones have also been developed using similar design. They can be arrayed and fixed undersea for constant monitoring. A different design avoids mechanical coupling with the seismic mass to improve the reproducibility of vibrational properties [30]. This seismometer is obtained with two reflectors on the opposite sides of the seismic mass (Fig. 4). A tunable diode couples light at 1.32 μm into a coupler that acts as beamsplitter. The two rays hit the seismic mass from opposite sides and back reflections are collected on the forth arm of the coupler. Vibration of the seismic mass will change the optical path in the two arms modifying the interference conditions at the detector. A triaxial system has been constructed using three identical mechanical receivers. This device is extremely compact (diameter <7cm, length~20cm) and can be coupled with optical fibre for remote sensing. A field test has been done showing an excellent reliability at 260 ^{o}C in the German Continental Deep Borehole at depth of about 8 km. Comparison between the results obtained with a standard broadband seismometer STS-2 and with the optical fibre seismometer showed an excellent agreement.

4.2 Intrinsic sensing

The majority of point intrinsic sensing is either based on microbending, EWS or FBG.

-Microbending

Microbending pressure devices are widely diffused intrinsic sensors. They consist of an optical fibre inserted between two plates with grooves interleaving with each other (fig. 5). If the sensor is not stimulated, the optical fibre is not bent (a) and the loss is negligible. If the fibre is bent there is a transmission loss associated with each bending (b). The mechanism of bending is presented in the bottom of fig. 5. The higher is the pressure on the plates, the greater the vertical movement of A and B in b). More loss consequently occurs because the light escapes from the core. A detector at the end of the fibre can detect the decrease in the intensity of the launched light. The device calibration then the measurement of the pressure on the plates. If fixed to rocks, this device can be used as a sensor for relative position and measure nanometric movements [31,32]. A system has been implemented to measure the growth in rock fissures. The optical fibre sensor is fixed to both the sides of the fissure so that the propagation loss will increase with increasing fissure opening. A calibration curve gives the relation between the observed loss, the number of bends and their spacing, the grooves curvature and the fissure growth. Many sensors can be arrayed to detect several sites simultaneously and monitored by an OTDR system (par. 3). The fault location is detected from the distance information obtained from the OTDR. This system can also be used for remote sensing [32]. Specific chemical sensors can also be produced using chemical sensitive materials that swell and induce bending losses in the fibre, such as using hydrogel polymers for detecting water [33].

-EWS

In the optical fibre the propagation mode is mainly contained in the core but there is still an evanescent part propagating into the cladding that is attenuated by the absorption of chemical compounds. Methane has an absorption peak at 1.66 μm and the attenuation at such wavelength allows the determination of methane concentration [34]. Many chemical sensors have a sensitive cladding that interacts with the optical fibre by means of the evanescent field. The absorption of the cladding changes when interacting with the chemical compound to detect. By detecting the change in the intensity launched into the fibre it is possible to detect the chemical concentration. Metallophthalocyanine thermally deposited at a reduced pressure can be used for NO_2 gas [35], polyoxyethylene for methane [36]. Extremely interesting for volcanic applications are CO_2 and H_2O sensors [28]. Thymol blue or phenolphthalein have been shown to be sensitive indicator dyes for CO_2, polyethylene oxide for moisture. Polyethylene is highly hygroscopic and has a refractive index lower than silica when dry, higher when impregnated with water. Hydrogen sulphide and oxide are also common compounds of geochemical interest. Hydrogen sulphide can be detected by a chemical agent containing lead acetate [37]. Unfortunately this is not a reversible sensor and the

device must be cleaned and recoated after each measurement. If a thermochromic compound is used as a cladding, guiding properties (thus output signal) are changed by temperature variations. Segmented polyurethane-diacetylene copolymer has been used for this kind of temperature EWS [38].

-FBG

FBG are narrow band reflectors that can be written into the guiding region of an optical fibre by UV beams [39]. The inscription of a periodic pattern in a photosensitive core is achieved by using UV lasers and is a quick and simple process. Moreover, FBG sensors have other advantages: immunity to electric and magnetic fields, high mechanical reliability, wavelength encoded operation, high temperature capabilities, minimal invasion in the measurement site, multiplexing, compatibility with devices developed for telecom applications, no electronics in the sensing place. Multiplexing is extremely important because it can provide 3D monitoring and simultaneous sensing of many parameters in many different locations [40]. Multiplexing is based on the use of many gratings working at different wavelengths. Each grating is defined by the wavelength at which its reflection is maximum (also called Bragg wavelength λ_B) and its maximum reflectivity (R), given by fabrication parameters according to following relations:

$$\lambda_B = \Lambda / 2n_{eff} \quad (5)$$

$$R = \tanh(\pi \Delta n_{mod} L / \lambda_B) \quad (6)$$

where Λ the grating pitch, n_{eff} effective refractive index (the refractive index averaged on the core mode distribution), Δn_{mod} in the refractive index modulation induced by UV exposure and L the grating length. The shift in λ_B ($\Delta\lambda_B$) is the mean of sensing. In fact Λ and n_{eff} are strictly related to temperature, pressure and strain and a simple calibration can connect an observed $\Delta\lambda_B$ with the respective temperature (T), pressure (P) or strain (ε) to be measured. Fig. 2 gives an example of calibration curve for T sensing over a broad range of temperatures. Typical values of calibration curves for the Bragg wavelength in silica fibres give a linear dependence for small perturbations: $\partial\lambda_B/\partial T \sim 0.01$ nm/^{O}C, $\partial\lambda_B/\partial P \sim 0.003$ nm/MPa, $1/\lambda_B \cdot \partial\lambda_B/\partial\varepsilon \sim 0.8$. Since gratings have different sensitivities at different wavelengths, two different gratings can be used to determine simultaneously the effects of strain and temperature [41]. Gratings are extremely good strain sensors and can be multiplexed [40] to monitor strains over a vast area. The detection is done with a spectrum analyser and the site is discriminated by λ_B. Multiplexing is in fact achieved using gratings with several different λ_B each of which corresponds to a sensor. In the microbending strain system proposed in 2.2.1 the propagation loss induced by a sensors affects the others in terms of

pumping power. A considerable growth in a rock fissure can induce such a high loss that back reflected signal cannot be detected by OTDR. On the contrary multiplexed FGB sensors are completely uncorrelated and even if a strain sensor monitors extremely high modifications, the sensitivity of the others remains unaffected. Conventional gratings written in germanosilicate or boro-germanosilicate fibres exhibit poor stability at high temperature, especially if hydrogen loaded [42]. High temperature FBG stability is required for sensing in harsh environments. For example, a strain sensor positioned in proximity of a volcanic area can easily be required to work above 400 ^{o}C. It is therefore necessary to optimise the fibre doping to achieve an enhanced thermal stability and excellent reliability of grating sensors. In the next section we show how gratings written in tin-doped silica fibres (SS) can be used up to a temperature of approximately 800 ^{o}C. At this temperature all the other gratings have been completely erased.

4.3 High temperature FBG

The SS fibre was fabricated via modified chemical vapour deposition [43] and had NA~0.1 and cut-off wavelength (λ_c)~1.3μm. Gratings were written using a KrF excimer laser delivering 20 ns pulses at 20 Hz. Pulse fluence was estimated to be ~100 mJ/cm^2. Gratings have also been written in germanosilicate (GS), boro-germanosilicate (BGS) and hydrogen loaded telecom (HLT) fibres. A grating written in tin-germanosilicate fibre was used as a reference for $\Delta\lambda_B$. The gratings were placed in a furnace. R was tested by monitoring with an optical spectrum analyser the light launched from a white light source and reflected by the grating via a coupler. The grating temperature was raised at a rate of ~25 °C/min, stabilised at working temperature for 4 hours and then decreased in steps to room temperature. Reflection spectra were recorded before each thermal step and at intervals of 15-60 mins at working temperature. Every cycle was repeated before increasing the working temperature in steps of 100 °C. Fig. 6 shows the temperature behaviour of the grating reflectivity. While HLT and BGS show an extremely poor stability and are completely erased at 500 ^{o}C in 4 hours, GS and SS present a better temperature dependence. In particular, gratings written in SS clearly exhibit the best thermal stability and cannot be erased by a thermal treatment at ~800 ^{o}C. Bragg gratings degradation shows a power-law function with time and the time constant of such decay is strongly dependent on T. While in most cases at room temperature the decay is just few percents over decades, at high temperatures an accelerate aging is observed and the grating can be completely erased in seconds. It has been shown [44] that accelerated aging performed at high temperature allows the prediction of grating behaviour at lower temperatures.

Due to his extremely high temperature stability, tin oxide results to be the best photosensitive doping for permanently installed high temperature grating devices.

5. Conclusions

The field of optical fibre distributed and point sensors has been reviewed with a particular emphasis for earth science applications. Fibre seismometer, thermometer, chemical and strain sensors have been described. Recent developments at Southampton University in long-range and high resolution spontaneous Brillouin-based distributed sensors and FBG sensors have been presented. A new Sn-doped optical fibre which exhibits high thermal accuracy and stability has been demonstrated.

6. References

[1] Gold MP, Design of a Long-range single-mode OTDR. J. Lightwave Tech. 1985; 3(1):39-46.

[2] MacLean A, Moran C, Thursby G, Pierce SG, Culshaw B, Graham NB. Distributed fiber optic sensors for humidity and hydrocarbon detection. Proc. of the SPIE 2000; 3986: 342-351.

[3] Barnowski MK, Jensen SM. Fiber waveguides: A novel technique for investigating attenuation characteristics. Appl. Opt. 1976; 15(9): 2112-2115.

[4] Personick SD. Photon-probe-An optical-fiber time domain reflectometer. Bell System Technical Journal 1977; 56(3): 355-366.

[5] Galeener FL, Mikkelsen JC, Geils RH, Mosby WJ. The relative Raman cross section of vitreous SiO_2,GeO_2, B_2O_3, and P_2O_5.Appl. Phys. Lett. 1978; 32(1): 34-36.

[6] Healey P. Fading in heterodyne OTDR. Electron. Lett. 1984; 20(1): 30-32.

[7] Kee HH, Lees GP, Newson TP. An all-fibre system for simultaneous interrogation of distributed strain and temperature sensing using spontaneous Brillouin scattering. Opt. Lett. 2000; 25(10): 695-697.

[8] Jones JDC. Review of fibre sensor techniques for temperature-strain discrimination. Tech. Dig. Optical Fiber Sensors 1997; 16: 36-39.

[9] Maughan SM, Kee HH, Newson TP. A 57-km single-ended spontaneous Brillouin-based distributed fiber temperature sensor using wideband microwave coherent detection. to be published in Opt. Lett.

[10] Hotate K, Hasegawa T. Measurement of Brillouin gain spectrum distribution along an optical fiber with a high spatial resolution using a novel correlation-base technique; demonstration of 45 cm spatial resolution. Tech. Dig. Optical Fiber Sensors 1999; 17: 337-340.

[11] Kee HH, Lees GP, Newson TP. Technique for measuring distributed temperature with 35 cm spatial resolution utilizing the Landau-Placzek ratio. IEEE Phot. Tech. Lett. 2000; 12(7): 873-875.

[12] Kee HH, Lees GP, Newson TP. An extended range OTDR system at 1.65 μm based on delayed Raman amplification. Opt. Lett. 1998; 23(5): 349-351.

[13] Kersey AD. Optical Fiber Sensors for Downwell Monitoring Applications in the Oil and Gas Industry. Tech. Dig. Optical Fiber Sensors 1999; 17: 326-329.

[14] Cox E, Jones B. Fiber optic color sensors based on Fabry-Perot interferometry. Proc. 1st Int. Conf. O.F.S. 1983; 122-126.

[15] Gerges AS, Newson TP, Jackson DA. Practical fiber-optic-based submicro-g accelerometer free from source and environmental perturbations. Opt. Lett. 1989; 14(20):1155-1157.

[16] Saaski E, Hartl J, Mitchell G. A fiber-optic sensing system based on spectral modulation. Proc. ISA/86 Int. Conf. (Houston, USA).

[17] Cartellier A. Optical probes for local void fraction measurements; characterization of performance. Rev. Sci. Instrum. 1990; 61: 874-886.

[18] Fernicola V, Crovini L. A high-temperature digital fiber-optic thermometer. Proc. 10th Int. Conf. O.F.S. 1994; 211-214.

[19] Noel B, Turley W, Lewis W, Tobin K, Beshears D. Phosphors thermometry on turbine-engine blades and vanes. In Temperature, Its Measurement and Control in Science and Industry, vol. 6, New York; 1249-54.

[20] Aizawa M, Okamoto T, Ono J, Araki Y, Nagai H. 30km long remote sensing of methane using a 1.65 μm DFB LD and single mode fiber. Proc. 9th Int. Conf. O.F.S. 1993; 285-288.

[21] Spencer JW, Smith SRW, Jones GR, Dean E, Simpson JCB. Optical fibre based groundwater sensor for monitoring land fill sites. Proc. SPIE 1997; 3105: 275-82.

[22] Bendamardji S, Alayli Y, Huard S, Remote CO_2 optical fibre sensor by molecular absorption at 4.3 μm. J. de Physique III 1996; 6(4): 491-503.

[23] Kobayashi T, Haruta M, Tsubota S, Sano H, Delmon B. Thin films of supported gold catalysts for CO detection. Sensors and Actuators B (Chemical) 1990; B1(1-6): 222-225.

[24] Buchholz F, Buschmann N, Cammann K. A fibre-optical sensor for the determination of sodium with a reversible response. Sensors and Actuators B (Chemical) 1992; B9 (1): 41-47.

[25] Wolfbeis OS, Weis LJ, Leiner MJP, Ziegler WE. Fiber-Optic Fluorosensor for Oxygen and Carbon Dioxide. Anal. Chem. 1988; 60: 2028-2030.

[26] Wolfbeis O, Sharma A. Fibre-optic fluorosensor for sulphur dioxide. Anal. Chim. Acta 1988; 208:53-58.

[27] Mizaikoff B, Gobel R, Krska R, Taga K, Kellner R, Tacke M, Katzir A. Infrared fiber-optical chemical sensors with reactive surface coatings. Sensors and Actuators B (Chemical) 1995; B29 (1-3):58-63.

[28] Gianfrani L, De Natale P, De Natale G. Remote sensing of volcanic gases with a DFB-laser-based fiber spectrometer. Appl. Phys. B 2000; 70(3): 467-470.

[29] Pechstedt RD, Jackson DA. Transducer mechanism of an optical fibre accelerometer based on a compliant cylinder design. Proc. 10th Int. Conf. O.F.S. 1994; 380-383.

[30] Ecke W, Schauer J, Willsch R. First field tests with the fiber optic high-temperature borehole seismometer. Proc. 12th Int. Conf. O.F.S. 1997; 630-633.

[31] Lagakos N. Microbend fiber optic sensor. Appl. Opt. 1987; 26: 2171.

[32] Kurii M, Ogata K, Yasuhara K, Katayose H, Nomura Y. Remote sensing system for a fissure in a rock using optical fiber. Proc. 14th Int. Conf. O.F.S. 2000; 768-771.

[33] Wallace P, Yang Y, Campbell M. Application of sol-gel processes for fibre optic chemical sensor development. Proc. 10th Int. Conf. O.F.S. 1994; 146-149.

Craig Michie W, Thursby G, McLean A, Culshaw B, Verwilghen B, Voet M, Fibre Optic Sensor for Distributed Water Ingress Detection and Humidity Measurement. Proc. 12th Int. Conf. O.F.S. 1997; 634-637.

[34] Culshaw B, Muhammad F, Steward G, Murray S, Pinchbeck D, Norris J, Cassidy S, Wilkinson M, Williams D, Crisp I, Van Ewyk R, McGhee A. Evanescent wave methane detection using optical fibres. Electron. Lett. 1992; 28(24): 2232-2234.

[35] John MS, Thomas J, Unnikrishnan KP, Radhakrishnan P, Nampoori VPN, Vallabhan CPG. NO_2 detection with a fibre optic evanescent wave sensor. Proc. SPIE 1999; 3897: 173-178.

[36] Archenault M, Gagnaire H, Goure JP, Jaffrezic-Renault N. A simple intrinsic optical-fibre chemical sensor. Sensors and Actuators B (Chemical) 1992; B8(2): 161-166.

[37] Jain SC, Singla ML, Singh N, Bhasin P, Singh M, Raj B, Aggarwal AK. An Intrinsic Fiber Optic H_2S Gas Sensor. Proc. 14th Int. Conf. OFS 2000; 416-419.

[38] Yuan J, El-Sherif MA. Development of on-fiber optical sensors utilizing chromogenic materials. Proc. SPIE 1999; 3538: 245-53.

[39] Meltz G, Morey WW, Glenn WH. Formation of Bragg gratings in optical fibres by a transverse holographic method. Opt. Lett. 1989; 14(15): 823-825.

[40] Dakin JP, Volanthen M. Distributed and Multiplexed Fibre Grating Sensors. Proc. 13th Int. Conf. OFS 1999; 134-140.

[41] Xu. M.G., Archambault J.L., Reekie L., Dakin J.P. Simultaneous Measurement of Strain and Temperature Using Fibre Grating Sensors. Proc. 10th Int. Conf. O.F.S. 1994; 191-194.

[42] Morey WW, Meltz G. High temperature capabilities and limitations of fiber grating sensors. Proc. 10th Int. Conf. O.F.S. 1994; 234-237.

[43] Brambilla G, Pruneri V, Reekie L. Photorefractive index gratings in SnO_2:SiO_2 optical fibers. Appl. Phys. Lett. 2000; 76: 807-809.

[44] Erdogan T, Mizrahi V, Lemaire PJ, Monroe D. Decay of ultraviolet-induced fiber Bragg gratings. J. Appl. Phys. 1994; 76(1):73-80.

7. Figure captions

Fig. 1(a). Experimental configuration for generating a high peak power, short pulse width source for single-ended spontaneous Brillouin-based distributed sensor.

Fig. 1(b). Sensor configuration for simultaneous strain and temperature measurement.

Fig. 2. Resolved profile along the sensing fibre for (a) strain distribution (b) temperature distribution

Fig. 3. Brillouin frequency shift dependence for various temperatures using the microwave heterodyne detection.

Fig. 4. Optical fibre seismometer [30]. The light emitted by the source diode is separated in two beams (dashed lines) in the 50/50 coupler and then reflected at the spherical reflectors. The two beams travel through some optics and recompose in the coupler. Their interference is recorded by the detector. Seismic motion of the mass will cause lateral motion of the reflectors and a change in the optical path difference between the two beams.

Fig. 5. A microbending sensor. The optical fibre is placed between two arms A and B. In a) the device is not stimulated and the fibre is not bent. When the sensor is detecting a variation in pressure or in position, the two arms move closer (b), the fibre is bent and an extra-loss is recorded.

Fig. 6. Temperature stability of gratings written in tin-silicate (SS), germanosilicate (GS), boro-germanosilicate (BGS) and hydrogen loaded telecom (HLT) fibres. Δn_{mod} and Δn_0 represents the refractive index modulations at temperature T and 20 ^{o}C respectively.

8. Figures

Fig. 1a

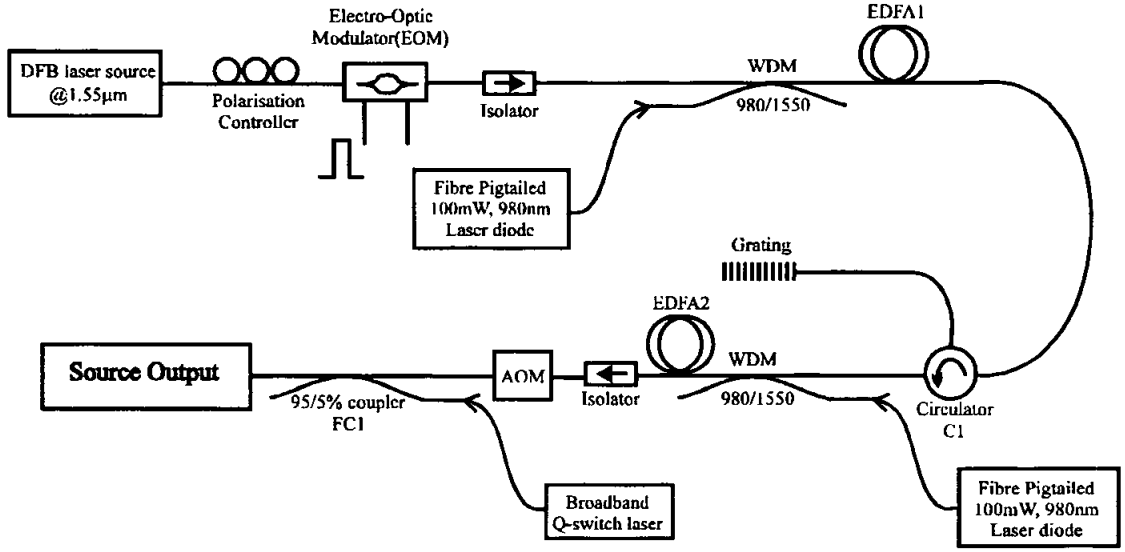

Fig. 1b

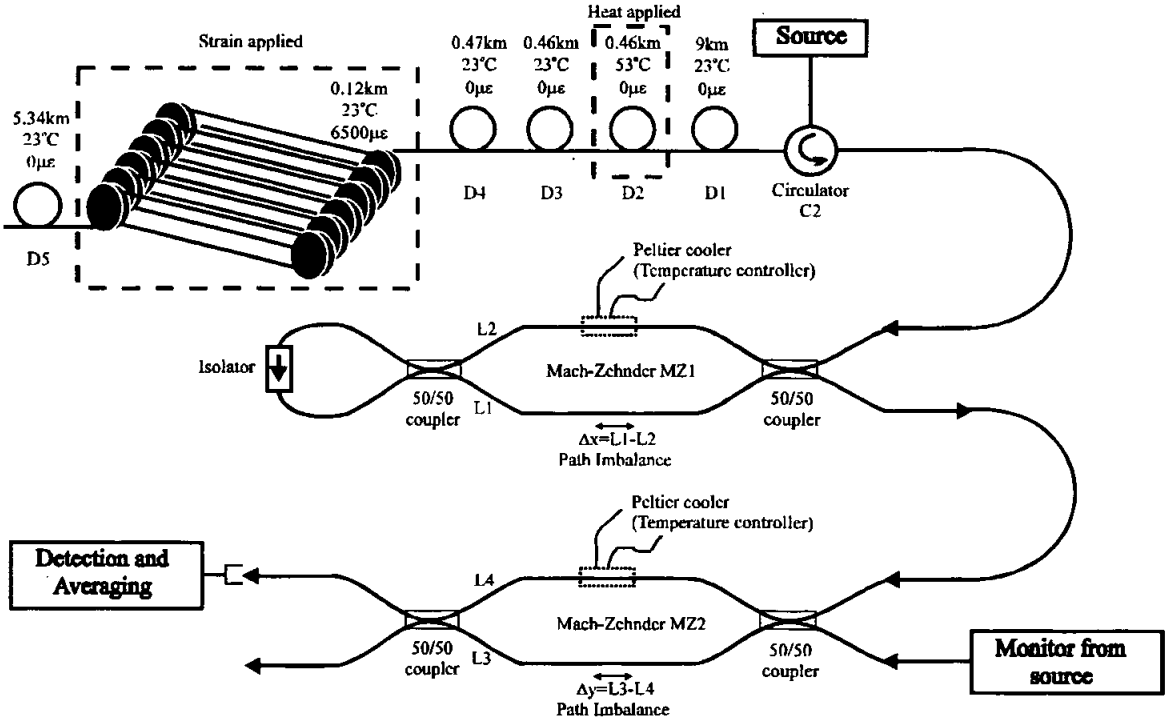

Fig. 2a

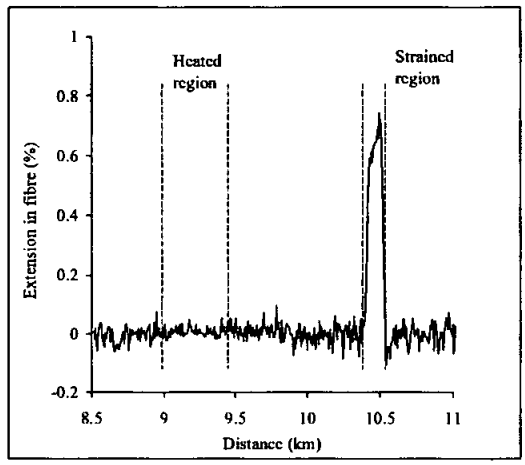
Heated region
Strained region
Extension in fibre (%)
1
0.8
0.6
0.4
0.2
0
-0.2
8.5
9
9.5
10
10.5
11
Distance (km)

Fig. 2b

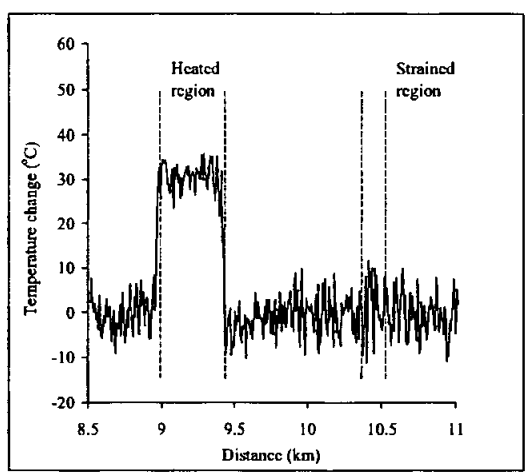
Heated region
Strained region
Temperature change (°C)
60
50
40
30
20
10
0
-10
-20
8.5
9
9.5
10
10.5
11
Distance (km)

Fig. 3

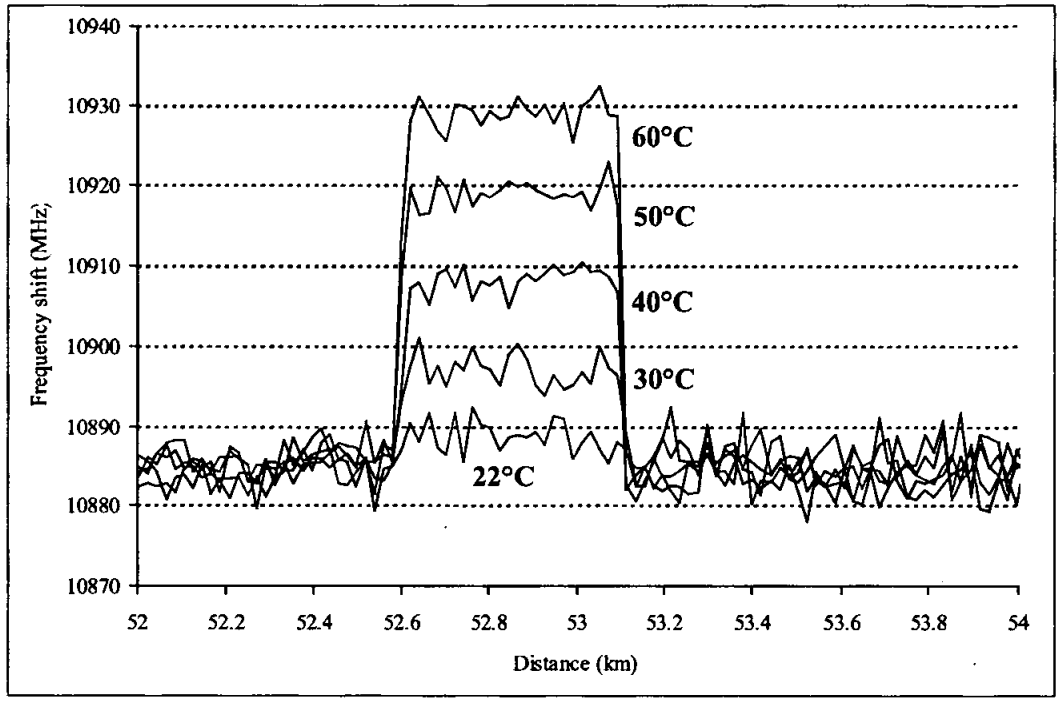
10940
10930
10920
10910
10900
10890
10880
10870
Frequency shift (MHz)
60°C
50°C
40°C
30°C
22°C
52
52.2
52.4
52.6
52.8
53
53.2
53.4
53.6
53.8
54
Distance (km)

Fig. 4

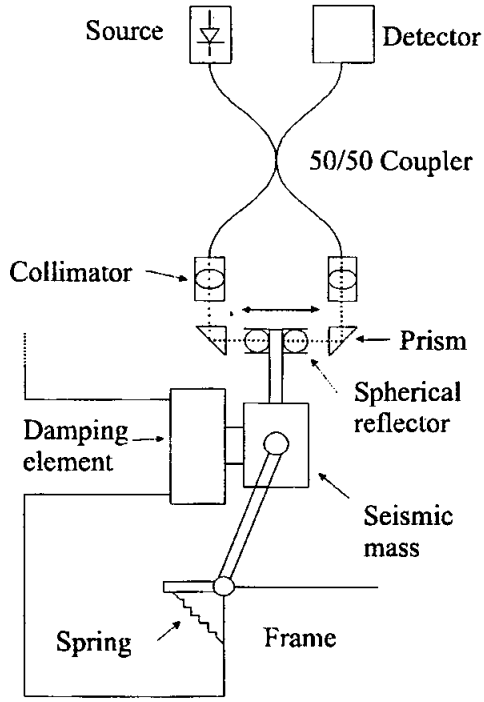
Source
Detector
50/50 Coupler
Collimator
Prism
Spherical reflector
Damping element
Seismic mass
Spring
Frame

Fig.5

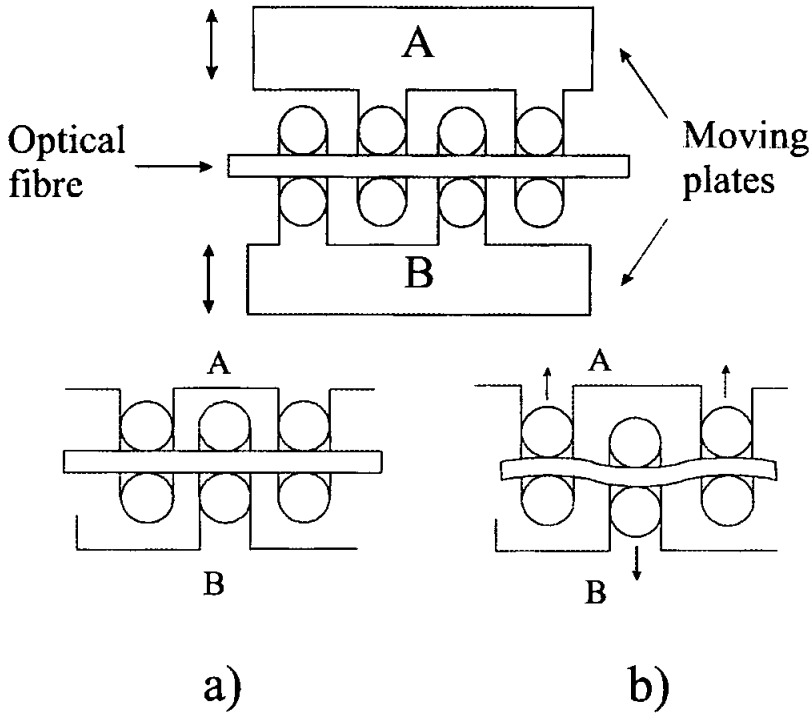
A
Optical fibre
Moving plates
B
A
B
A
B
a)
b)

Fig. 6

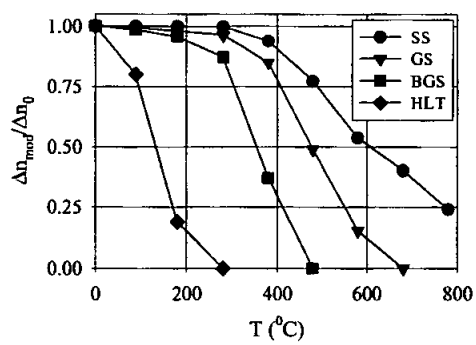
1.00
0.75
0.50
0.25
0.00
0
200
400
600
800
T (°C)
SS
GS
BGS
HLT